



Massively distributed fiber strain sensing using Brillouin lasing

JOSEPH B. MURRAY,^{1,*}  ALEXANDER CERJAN,²  AND BRANDON REDDING¹ 

¹*U.S. Naval Research Laboratory, 4555 Overlook Ave. SW, Washington, DC 20375, USA*

²*Center for Integrated Nanotechnologies, Sandia National Laboratories, Albuquerque, New Mexico 87123, USA*

**joseph.murray@nrl.navy.mil*

Abstract: Brillouin based distributed fiber sensors present a unique set of characteristics amongst fiber sensing architectures. They are able to measure absolute strain and temperature over long distances, with high spatial resolution, and very large dynamic range in off-the-shelf fiber. However, Brillouin sensors traditionally provide only modest sensitivity due to the weak dependence of the Brillouin frequency on strain and the high signal to noise ratio required to identify the resonance's peak frequency to within a small fraction of its linewidth. Recently, we introduced a technique which substantially improves the precision of Brillouin fiber sensors by exciting a series of lasing modes in a fiber loop cavity that experience Brillouin amplification at discrete locations in the fiber. The narrow-linewidth and high intensity of the lasing modes enabled ultra-low noise Brillouin sensors with large dynamic range. However, our initial demonstration was only modestly distributed: measuring strain at 40, non-contiguous positions along a 400 m fiber. In this work, we greatly extend this methodology to enable fully distributed sensing at 1000 contiguous locations along 3.5 km of fiber—an order of magnitude increase in sensor count and range. This highly-multiplexed Brillouin fiber laser sensor provides a strain noise as low as $34 \text{ n}\epsilon/\sqrt{\text{Hz}}$ and we analyze the limiting factors in this approach.

© 2022 Optica Publishing Group under the terms of the [Optica Open Access Publishing Agreement](#)

1. Introduction

Brillouin based fiber sensors have advanced considerably in the three decades since their first inception [1,2]. The growth of this technology has led to a broad range of sensor architectures optimized for long range [3–7], high resolution [8–11], high speed operation [12–16], and wide dynamic range [14,17–20] all using commercial off-the-shelf fiber. Despite variations in their approach, all of these sensors are designed to measure the Brillouin frequency shift (BFS), which is a linear function of strain and temperature. Although this sensing modality has been substantially refined, it is still hampered by the inherently low sensitivity of the Brillouin frequency to temperature or strain. As such, achieving low strain uncertainty requires Brillouin sensors to identify changes in the Brillouin resonance that are a small fraction of the Brillouin linewidth.

Recently, we demonstrated a substantial enhancement of the precision in determining the Brillouin frequency using the excitation of a series of Brillouin lasing modes within the fiber [20]. Our scheme relied on periodically pumping a fiber ring cavity such that the pump period matches the round-trip time in the cavity, exciting a series of narrowband lasing modes that experience Brillouin amplification at discrete locations in the fiber under test (FUT). In some ways, this scheme is similar to a standard Brillouin optical time domain reflectometer (BOTDR) [21], in which a pump pulse enters the FUT and the system measures the frequency of the backscattered light over time. However, instead of measuring the frequency of weak, spectrally broad, spontaneously backscattered light from each position in the fiber, the Brillouin laser sensor measures the frequency of a train of lasing modes. Since these lasing modes are both brighter

and spectrally narrower than spontaneous Brillouin scattered light, the Brillouin laser sensor enables a far more accurate measurement of the Brillouin frequency.

In practice, the approach presented in [20] had a few limitations. First, in order to avoid interference between neighboring lasing modes, the sensor positions were spatially separated, resulting in a sparse measurement covering only 40% of the fiber under test. Second, the initial demonstration was limited to 40 lasing modes in only 400 m of fiber, and it was unclear if mode competition, pump depletion, and attenuation would prevent highly distributed sensing over longer range.

Here, we present a technique that enables a fully distributed measurement probing every position in a fiber. This is accomplished by circulating two sets of lasing modes, each of which cover half the sensing positions in the FUT. These modes are then computationally interleaved, resulting in complete coverage of the FUT at the cost of a 2x reduction in bandwidth. Further, we demonstrate the scalability of this approach by exciting 1000 lasing modes along the last 3.5 km of a 5 km fiber while maintaining a low strain noise ($34 \text{ n}\epsilon/\sqrt{\text{Hz}}$) and a large dynamic range ($\sim 5 \text{ m}\epsilon$). Finally, we show that the limits on range and sensitivity are not specific to this scheme, but are instead given by the onset of modulation instability.

2. Approach

The sensor is designed to excite a series of pulsed lasing modes that circulate in a fiber ring cavity and experience Brillouin amplification at the same position in the fiber after each round trip. This can be achieved by introducing a pulsed pump with a repetition period matched to the round-trip time in the cavity. The FUT forms approximately half of the cavity where the lasing modes interact with the pump. A slightly longer section is used to delay the modes, ensuring that each lasing mode only interacts with the pump pulse at one position in the FUT (i.e., the pump pulse should leave the FUT section of the ring before the first lasing mode is coupled back into the FUT). Since the spatial extent of the pulsed lasing modes is shorter than the cavity length, the lasing frequency is not dictated by the resonant modes of the cavity. Instead, the modes lase at the frequency that experiences the most gain, corresponding to the peak of the Brillouin gain spectrum at the position in the fiber where a given mode is amplified. This is crucial since it ensures that the lasing frequencies are insensitive to phase variations in the optical pathlength of the cavity. Thus, by measuring the frequency of the circulating lasing modes, the sensor is able to infer the Brillouin frequency as a function of position in the fiber.

We encountered two related challenges when implementing this scheme. First, coupling and interference between partially overlapping lasing modes corrupted the frequency measurements and introduced cross-talk between nearby positions in the fiber. Second, mode competition for gain limited the number of lasing modes which could be excited at once. To overcome these challenges, we introduced an intensity modulator in the cavity. To avoid interference between overlapping lasing modes, transmission through the modulator was pulsed so that neighboring lasing modes were temporally (and spatially) separated. The modulator was also used to compensate for mode competition, by adjusting the loss experienced by each mode. While this allowed us to excite a series of discrete lasing modes, the modes were spatially separated, resulting in a quasi-distributed measurement at a series of non-contiguous positions. In addition, our initial demonstration was limited to 40 lasing modes (i.e., 40 sensor positions). It was unclear if this approach could be scaled to more modes and longer sensing fiber lengths since mode competition, pump depletion, and attenuation could all be limiting factors.

In this work, we adjusted the control scheme to excite two sequences of lasing modes. The length of the cavity was increased to store an extra train of lasing modes while the pump period was set to half the round-trip time. We then used the intra-cavity modulator to define the lasing positions so that the “odd” positions in the fiber were probed using the first sequence of lasing

modes and “even” positions with the second sequence. This allowed for fully-distributed sensing at every position in the fiber.

Figure 1 schematically shows the architecture and control scheme used in this work. A single narrow linewidth laser (<1 kHz) is split into the pump and LO paths. Along the pump path, the laser was first directed to an acousto-optic modulator (AOM) driven by a short RF burst. This provides high extinction, but the pulse lengths are limited to ~ 100 ns. EOM_1 then carves 40 ns pulses with modest extinction (setting the measurement resolution to 4 m; see Supplement 1 for a discussion of spatial resolution). The pump pulse repetition period was set to half the round-trip time in the cavity (within 0.5 ns) in order to excite two sequences of lasing modes. Note that the system is robust to slight mismatches between the pulse repetition period and half the round-trip cavity length (up to a few ns), which will introduce small amounts of additional loss. In this work, the repetition period was set to 51.4 μ s since the cavity length was ~ 20 km (including a 5 km FUT and 15 km feedback fiber). The pump pulses are then directed to a polarization switch consisting of a 2×2 EOM and a polarizing beam splitter (PBS). The EOM directed alternating pulses to opposite ports of the PBS, producing sequential pump pulses with orthogonal polarization to mitigate polarization fading. Finally, the pump pulses were amplified by an erbium doped fiber amplifier (EDFA) and injected into the fiber under test (FUT) section of the ring cavity through a circulator. A second circulator was used to remove the residual pump pulse at the end of the FUT, enabling non-resonant pumping. Note that both EDFAs used in this study include a 100 GHz wavelength division multiplexing (WDM) filter to reduce the amplified spontaneous emission (ASE). For this work the peak pump power was set to the maximum before the onset of significant modulation instability (~ 1 W).

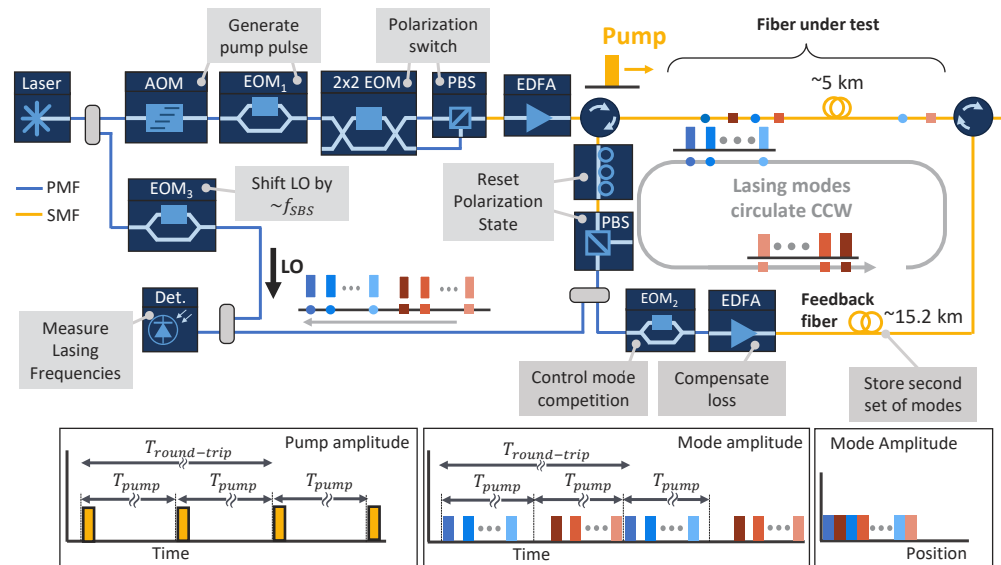


Fig. 1. The experimental setup used to realize the fully distributed Brillouin fiber laser sensor. The fiber ring consists of a ~ 5 km section of fiber under test as well as a ~ 15 km feedback fiber. The longer section of feedback fiber allows two sets of modes to circulate in the cavity. One set of modes (blue) measures the odd positions in the fiber, while the other set (orange) is offset from the first such that it probes the even positions. Pump pulses are introduced at a period equal to half the round-trip time in the fiber ring cavity. After demodulation, the measurements can be interleaved to retrieve the Brillouin frequency shift at every position.

The fiber ring cavity consists of the FUT, polarization control, amplitude control, amplification, and delay sections. The FUT (the upper part of the fiber ring cavity in Fig. 1) consists of a 5 km fiber, including 4 m on a linear strain stage and ~4 m on a temperature control stage. A set of polarization control paddles and a polarizing beam splitter are used to reset the polarization state of the modes after each round-trip to prevent polarization procession [20]. A 90:10 coupler directs a small portion of the circulating lasing modes to the detector where it is combined with the LO to measure the lasing frequency. The other 90% of the light is directed to EOM₂, which was used to define the lasing positions and compensate for mode competition. EOM₂ was driven with two sequences of 500 pulses. Each pulse was 40 ns long (matching the pump pulse duration) and the pulses were separated by 72 ns (resulting in 7.2 m mode spacing). By temporally separating the lasing modes in each sequence, we prevent inter-mode interaction such as mode coupling, as well as interference between neighboring modes which could corrupt the frequency measurement. The two sequences were offset by 36 ns relative to the two pump pulses that entered the FUT each round trip. The pulses were timed such that the lasing modes probed the last 3.5 km of the 5 km FUT. As shown in the timing diagram in the lower inset in Fig. 1, this resulted in two sequences of lasing modes which experienced Brillouin amplification at interleaved “odd” and “even” positions in the FUT. To compensate for mode competition and ensure single-mode lasing at each sensor position, an automated routine was used to adjust the transmission through EOM₂ for each pulse [20]. This ensured that each lasing pulse consisted of light at a single frequency, albeit transform-limited by the pulse duration.

After EOM₂, the lasing modes were directed to an EDFA which compensated for loss in the cavity and reduced the Brillouin pump power required to achieve lasing. Finally, a 15.2 km “feedback” section of the fiber cavity was used to delay the lasing modes before they are coupled back into the FUT. Note that the first and last modes excited by a given pump pulse will be separated by the round-trip time in the FUT. Spatially, these modes will be separated by twice the length of the FUT. In order to accommodate two sets of lasing modes, the entire cavity needs to be 4x the length of the FUT—achieved by setting the feedback section to be at least 3x longer than the FUT. This ensures that the “odd” sequence of lasing modes will not interact with the pump pulse intended for the “even” sequence of lasing modes and vice versa.

To measure the lasing frequency, we combined the lasing modes with a LO using heterodyne detection. The LO was directed through EOM₃, which was driven at approximately the Brillouin frequency (~10.8 GHz) in the suppressed carrier mode to create a pair of sidebands. The lasing modes and LO were then combined on an 800 MHz detector and the interference signal was digitized at 1 GS/s. We used I/Q demodulation to extract the amplitude and phase of the lasing modes and recovered the frequencies of the lasing modes by linear regression of the slope of the demodulated phase [20]. Finally, the measurements obtained from the two sequences of lasing modes are interleaved to obtain a continuous measurement of the Brillouin frequency as a function of position in the FUT.

It should be noted that, while this interleaving approach enables completely distributed sensing, it does entail some trade-offs. Most importantly, this scheme doubles the sensor density at the cost of halving the sensor bandwidth and thus increasing the sensor self-noise by a factor of $\sqrt{2}$. However, since this technique does not require scanning or averaging to obtain a measurement, the sensor bandwidth remains relatively high. The other trade-off is that the feedback fiber needs to be 3x the length of the FUT, rather than simply equal to the length of the FUT. This could be a more significant drawback at longer ranges due to optical attenuation.

3. Experiments

Figure 2 shows the basic operation of the system and the computational interleaving. A typical interference signal recorded on the photodetector is shown in Fig. 2(a). This interference signal includes two sequences of 500 lasing modes. The round-trip time in the fiber ring is 102.8 μ s

and the pump repetition period was set to $51.4 \mu\text{s}$. The first set of modes (blue) probes the “even” fiber positions while the second set (orange) probes the “odd” fiber positions. As shown in Figs. 2(b),(c), the individual lasing modes are confined to $\sim 40 \text{ ns}$ and spaced by 72 ns , matching the settings on EOM₂. This separation was chosen to provide a slight overlap between the sensor positions probed by the “odd” and “even” modes. This overlap is evident in Fig. 2(d), which shows the same modes in Figs. 2(b),(c), but converted to position in the fiber.

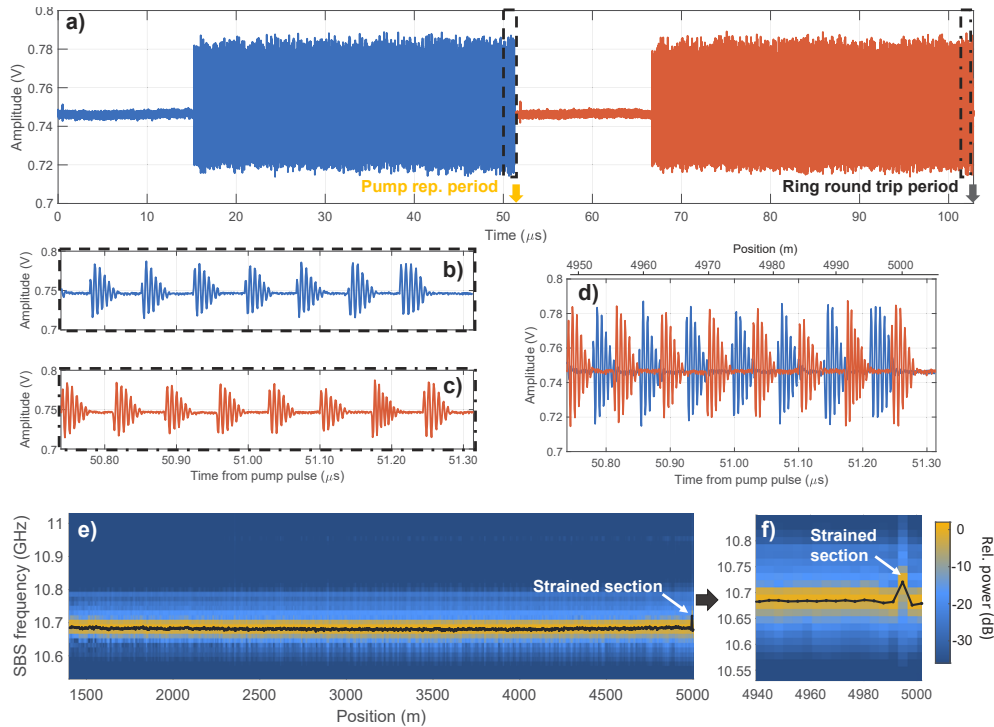


Fig. 2. Experimental demonstration of the fully distributed fiber laser sensing technique. (a) A typical time trace of the interference pattern produced by the mixing of the LO and the 1000 lasing modes over a complete round trip period of the fiber ring cavity. This includes two sets of modes: the first set (blue) probes the “odd” positions in the FUT while the second set (orange) measures the “even” positions in the FUT. (b),(c) The interference patterns of the last few modes in each set, with the time referenced to the introduction of the pump pulse. (d) The interference patterns from (b),(c) overlapped, showing that by interleaving the two sets of modes, every position is measured. (e) Spectrogram depicting the Fourier transform of the interleaved modes. The black line marks the peak at each position. The inset (f) shows the last 60 m of FUT where a 4 m section of fiber is under strain. The frequency in the strained section is shifted by $\sim 40 \text{ MHz}$ while the surrounding modes are unaffected.

Figure 2(e) shows a spectrogram obtained by calculating the Fourier transform of each lasing mode. The linewidths of the individual modes are transform limited to $\sim 25 \text{ MHz}$ based on the 40 ns pump pulses. The peak of the spectrogram is marked with a black line. Note that the spectrogram is for illustrative purpose—in practice, the Brillouin frequencies were extracted by measuring the slope of the demodulated phase of each mode. Nonetheless, this spectrogram provides a clear visualization of the sensor operation. The FUT consists of a 5 km spool of fiber with a 4 m section of fiber near the end wrapped on a linear strain stage. In this case the 3rd from the last mode probes the section of fiber on the stage. As can be seen in Fig. 2(f) the frequency of this mode was shifted by $\sim 40 \text{ MHz}$ due to the applied strain. However, the surrounding modes

remain unaffected confirming that the “odd” and “even” modes probe distinct positions along the fiber. This represents a substantial improvement over our previous work, which effectively only probed the odd modes, and thus would have “missed” this strained section.

The sensor was then quantitatively characterized by measuring the frequency response of the lasing modes to changes in temperature or strain. Figure 3 plots the measured change in the Brillouin frequency for an odd lasing mode near the beginning of the FUT (mode number 11, positioned ~ 1500 m into the FUT), an even mode sensing the middle of the fiber (mode number 502, sensing ~ 3100 m into the FUT), and a mode sensing the strained region at the end of the FUT (mode number 998, sensing 4993 m into the FUT) while the strain was swept from 0 strain to >4 m ϵ . Here the maximum measured strain is limited by our strain stage, whereas the dynamic range of the sensor is limited only by the bandwidth of the detector and digitizer (350 MHz, corresponding to a dynamic range of ~ 7 m ϵ). These measurements took place over ~ 1 hr. Over this time period, the measured Brillouin frequency drifted with a standard deviation of ~ 1 MHz. We found that this drift was primarily due to changes in the lasing amplitude and amplitude-to-frequency cross-sensitivity in the demodulation algorithm. After compensating for this effect, the fluctuations were suppressed, resulting in the measurement shown in Fig. 3. The modified algorithm used to remove the amplitude cross-sensitivity is discussed in Supplement 1.

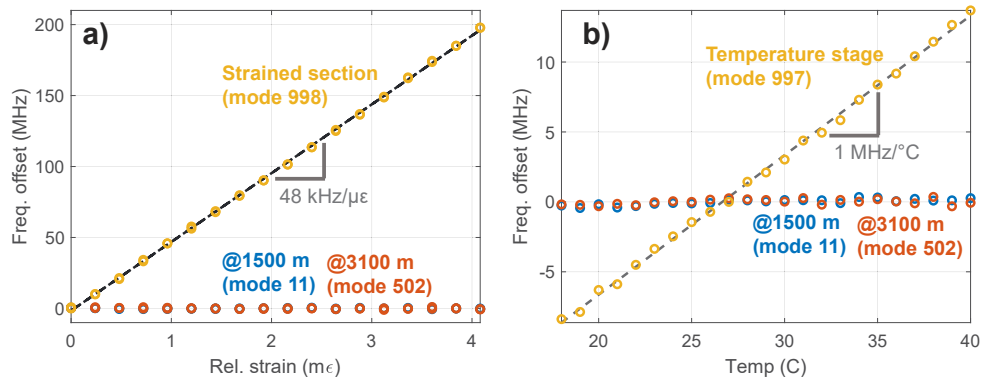


Fig. 3. (a) Measured frequency offset versus applied strain in the 4m section of strained fiber near the end of the FUT. An odd mode near the start of the FUT (mode 11, ~ 1500 m into the FUT) and an even mode in the middle of the FUT (mode 502, ~ 3100 m into the FUT) are also shown. The sensor at the strained position accurately measures the strain with excellent linearity while crosstalk at the other lasing positions is below the noise level. (b) The measured frequency shift versus temperature shift in a section of fiber on a temperature stage near the end of the FUT along with two reference positions. The frequency shift due to temperature is accurately recovered in the mode at the heated/cooled position without cross-talk.

As can be seen, the laser sensor in the strain section experienced a linear change in frequency with a slope of 48.5 kHz/ $\mu\epsilon$, in good agreement with the nominal strain sensitivity of ~ 50 kHz/ $\mu\epsilon$ for Brillouin fiber sensors [22]. Similarly, a section near the end of the FUT was placed on a temperature control stage and the temperature was swept from 18 to 40 °C. Figure 3(b) displays the frequency of the lasing mode probing the temperature-controlled section compared to the same modes shown in Fig. 3(a). The frequency response of the temperature modulated sensor was 1.00 MHz/ $^{\circ}\text{C}$ in excellent agreement with the nominal dependence of ~ 1 MHz/ $^{\circ}\text{C}$ [22]. In both sweeps, cross talk between the modulated section and the other modes was below the noise level and suppressed by at least a factor of 200.

We then investigated the noise dependence of the sensor as a function of mode number and pump power. To do this, we recorded a series of datasets while varying the peak pump power

from 620 mW to 1140 mW. As the Brillouin pump power increased, we reduced the EDFA gain in the loop to prevent multimode lasing. We also allowed the automated routine to re-balance the transmission through EOM₂ to obtain single mode lasing at all sensor positions at each pump power. We then calculated the minimum detectable strain for each sensor position. Figure 4(a) shows the measured noise of the sensor versus position for each pump power. At low pump powers, the noise was relatively high since a large portion of the gain is provided by the EDFA, resulting in broadband noise. As the pump power increases, the noise uniformly decreases until it reaches a minimum of 34 nε/√Hz (with average noise of 52 nε/√Hz) at a pump power of ~1.03 W. However, continuing to increase the pump power to 1140 mW introduced a sharp increase in noise at the end of the fiber. This noise increase stems from modulation instability which eventually decreases the power at the original pump frequency, as confirmed by monitoring the transmitted pump spectrum on an optical spectrum analyzer (see Supplement 1).

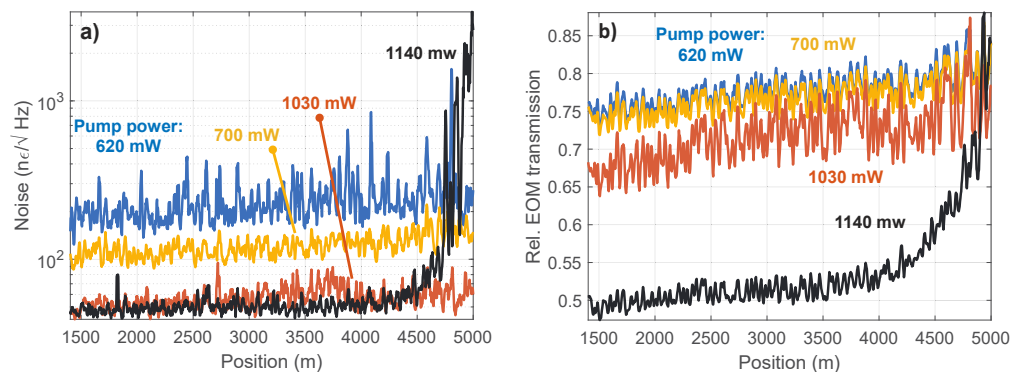


Fig. 4. The variation in sensor noise and loop EOM transmission required for lasing. (a) The measured noise versus sensor position for several peak pump powers. The noise decreases with increasing pump power until ~1 W, after which modulation instability reduces the available pump power for modes near the end of the FUT. (b) The relative EOM transmission required for each mode to produce lasing. At high pump powers, the transmission for the modes near the end of the FUT needs to be greatly increased since modulation instability reduces the pump power available at the original pump frequency at the end of the FUT.

This effect can also be seen in the calculated transmission through EOM₂ which was optimized in an automated feedback loop to ensure that each mode lases with uniform power without the onset of multimode lasing. Figure 4(b) shows the relative EOM transmission vs sensor position for various peak pump powers. At low pump powers, the transmission is relatively uniform for all of the modes. The slight increase in transmission with position is attributed to gain saturation effects in the EDFA, rather than depletion of the Brillouin pump. Since the lasing modes entering the FUT had a peak power of ~1 mW, pump depletion was relatively minimal (see Supplement 1). However, the EOM transmission changed dramatically at a pump power of 1140 mW, and much higher transmission was required to obtain lasing at the end of the fiber. This is consistent with reduced Brillouin gain at the end of the fiber due to modulation instability.

As in most distributed fiber sensors, increasing the length of the FUT reduces the sensor bandwidth and increases the self-noise since the measurement rate is reduced. Since the modulation instability threshold also depends on the fiber length, increasing the fiber length will require a reduction in pump power which will also increase the self-noise.

Lastly, the uniform strain noise across 1000 modes in Fig. 4(a) confirms that we were able to excite single mode lasing at 1000 positions simultaneously. We were initially concerned that it would be challenging to optimize the transmission through EOM₂ for 1000 modes simultaneously. However, as the number of modes increases the influence of a single mode amplitude is diminished.

While the system has more degrees of freedom it is more robust to perturbations. Thus, we found that the same iterative algorithm described in [20] which adjusts the transmission for all modes at once rapidly converged despite the large number of modes (typically requiring only a few seconds). Overall, the mode balancing process does not appear to become significantly more challenging as the number of modes increases.

4. Conclusions

Here, we introduced a technique which allows for continuously distributed sensing using Brillouin lasing. We also demonstrated the scalability of this approach, showing operation in 3.5 km of fiber with 1000 sensing positions. We investigated the pump power dependence and found that modulation instability eventually limits the sensor performance, similar to other Brillouin sensing techniques. However, this limitation in noise performance/range also implies that the system is amenable to further improvements using techniques such as distributed Raman amplification.

Funding. National Nuclear Security Administration (DE-NA-0003525); U.S. Naval Research Laboratory.

Acknowledgments. This work was supported by the U.S. Naval Research Laboratory.

A.C. recognizes the support of the Laboratory Directed Research and Development (LDRD) program and the Center for Integrated Nanotechnologies, an Office of Science User Facility operated for the U.S. Department of Energy (DOE) Office of Science. Sandia National Laboratories is a multimission laboratory managed and operated by National Technology & Engineering Solutions of Sandia, LLC, a wholly owned subsidiary of Honeywell International, Inc., for the U.S. DOE's National Nuclear Security Administration under contract DE-NA-0003525. The views expressed in the article do not necessarily represent the views of the U.S. DOE or the United States Government.

Disclosures. J.M. and B. R. declare U.S. Patent (Application No. 17400107).

Data availability. Data underlying the results presented in this paper are not publicly available at this time but may be obtained from the authors upon reasonable request.

Supplemental document. See [Supplement 1](#) for supporting content.

References

1. T. Kurashima, T. Horiguchi, and M. Tateda, "Distributed-temperature sensing using stimulated Brillouin scattering in optical silica fibers," *Opt. Lett.* **15**(18), 1038–1040 (1990).
2. T. Horiguchi, T. Kurashima, and M. Tateda, "A technique to measure distributed strain in optical fibers," *IEEE Photonics Technol. Lett.* **2**(5), 352–354 (1990).
3. X. H. Jia, Y. J. Rao, L. Chang, C. Zhang, and Z. L. Ran, "Enhanced sensing performance in long distance Brillouin optical time-domain analyzer based on Raman amplification: Theoretical and experimental investigation," *J. Lightwave Technol.* **28**(11), 1624–1630 (2010).
4. A. Dominguez-Lopez, A. Lopez-Gil, S. Martin-Lopez, and M. Gonzalez-Herraez, "Strong cancellation of RIN transfer in a Raman-assisted BOTDA using balanced detection," *IEEE Photonics Technol. Lett.* **26**(18), 1817–1820 (2014).
5. Y. Dong, L. Chen, and X. Bao, "Time-division multiplexing-based BOTDA over 100 km sensing length," *Opt. Lett.* **36**(2), 277–279 (2011).
6. M. A. Soto, M. Taki, G. Bolognini, and F. Di Pasquale, "Simplex-coded BOTDA sensor over 120-km SMF with 1-m spatial resolution assisted by optimized bidirectional Raman amplification," *IEEE Photonics Technol. Lett.* **24**(20), 1823–1826 (2012).
7. M. A. Soto, G. Bolognini, and F. Di Pasquale, "Long-range simplex-coded BOTDA sensor over 120 km distance employing optical preamplification," *Opt. Lett.* **36**(2), 232–234 (2011).
8. A. W. Brown, B. G. Colpitts, and K. Brown, "Dark-Pulse Brillouin Optical Time-Domain Sensor With 20-mm Spatial Resolution," *J. Lightwave Technol.* **25**(1), 381–386 (2007).
9. Y. Dong, H. Zhang, L. Chen, and X. Bao, "2 cm spatial-resolution and 2 km range Brillouin optical fiber sensor using a transient differential pulse pair," *Appl. Opt.* **51**(9), 1229–1235 (2012).
10. A. Bergman, T. Langer, and M. Tur, "Coding-Enhanced Ultrafast and Distributed Brillouin Dynamic Gratings Sensing Using Coherent Detection," *J. Lightwave Technol.* **34**(24), 5593–5600 (2016).
11. K. Y. Song, Z. He, and K. Hotate, "Distributed strain measurement with millimeter-order spatial resolution based on Brillouin optical correlation domain analysis and beat lock-in detection scheme," *Opt. InfoBase Conf. Pap.* **31**(17), 2526–2528 (2006).
12. J. B. Murray and B. Redding, "Combining Stokes and anti-Stokes interactions to achieve ultra-low noise dynamic Brillouin strain sensing," *APL Photonics* **5**(11), 116104 (2020).

13. C. Jin, L. Wang, Y. Chen, N. Guo, W. Chung, H. Au, Z. Li, H.-Y. Tam, and C. Lu, "Single-measurement digital optical frequency comb based phase-detection Brillouin optical time domain analyzer," *Opt. Express* **25**(8), 9213–9224 (2017).
14. A. Voskoboinik, A. E. Willner, and M. Tur, "Extending the Dynamic Range of Sweep-Free Brillouin Optical Time-Domain Analyzer," *J. Lightwave Technol.* **33**(14), 2978–2985 (2015).
15. Y. Peled, A. Motil, L. Yaron, and M. Tur, "Slope-assisted fast distributed sensing in optical fibers with arbitrary Brillouin profile," *Opt. Express* **19**(21), 19845–19854 (2011).
16. J. B. Murray and B. Redding, "Suppressing non-local effects due to Doppler frequency shifts in dynamic Brillouin fiber sensors," *Opt. Express* **28**(8), 10760–10771 (2020).
17. G. Yang, X. Fan, and Z. He, "Strain dynamic range enlargement of slope-assisted BOTDA by using Brillouin phase-gain ratio," *J. Lightwave Technol.* **35**(20), 4451–4458 (2017).
18. D. Zhou, Y. Dong, B. Wang, T. Jiang, D. Ba, P. Xu, H. Zhang, Z. Lu, and H. Li, "Slope-assisted BOTDA based on vector SBS and frequency-agile technique for wide-strain-range dynamic measurements," *Opt. Express* **25**(3), 1889–1902 (2017).
19. Z. Yang, M. A. Soto, D. M. Chow, P. Ray, and L. Thevenaz, "Brillouin Distributed Optical Fiber Sensor Based on a Closed-Loop Configuration," *J. Lightwave Technol.* **36**(5), 1239–1248 (2018).
20. J. Murray, A. Cerjan, and B. Redding, "Distributed Brillouin fiber laser sensor," *Optica* **9**(1), 80–87 (2022).
21. Q. Bai, Q. Wang, D. Wang, Y. Wang, Y. Gao, H. Zhang, M. Zhang, and B. Jin, "Recent advances in Brillouin optical time domain reflectometry," *Sensors* **19**(8), 1862 (2019).
22. A. Motil, A. Bergman, and M. Tur, "[INVITED] State of the art of Brillouin fiber-optic distributed sensing," *Opt. Laser Technol.* **78**, 81–103 (2016).